

Flash-Unified: A Training-Free and Task-Aware Acceleration Framework for Native Unified Models

Junlong Ke^{2*} Zichen Wen^{1,3*} Boxue Yang¹ Yantai Yang¹ Xuyang Liu^{1,4} Chenfei Liao⁵
 Zhaorun Chen⁶ Shaobo Wang¹ Linfeng Zhang^{1†}
¹ Shanghai Jiao Tong University ² Tsinghua University ³ Shanghai AI Laboratory
⁴ Sichuan University ⁵ The Hong Kong University of Science and Technology (Guangzhou)
⁶ University of Chicago

Abstract

Native unified multimodal models, which integrate both generative and understanding capabilities, face substantial computational overhead that hinders their real-world deployment. Existing acceleration techniques typically employ a static, monolithic strategy, ignoring the fundamental divergence in computational profiles between iterative generation tasks (e.g., image generation) and single-pass understanding tasks (e.g., VQA). In this work, we present the first systematic analysis of unified models, revealing pronounced parameter specialization, where distinct neuron sets are critical for each task. This implies that, at the parameter level, unified models have implicitly internalized separate inference pathways for generation and understanding within a single architecture. Based on these insights, we introduce a training-free and task-aware acceleration framework, **FlashU**, that tailors optimization to each task’s demands. Across both tasks, we introduce *Task-Specific Network Pruning and Dynamic Layer Skipping*, aiming to eliminate inter-layer and task-specific redundancy. For visual generation, we implement a time-varying control signal for the guidance scale and a temporal approximation for the diffusion head via *Diffusion Head Cache*. For multimodal understanding, building upon the pruned model, we introduce *Dynamic Token Pruning* via a *V-Norm Proxy* to exploit the spatial redundancy of visual inputs. Extensive experiments on *Show-o2* demonstrate that *FlashU* achieves $1.78\times$ to $2.01\times$ inference acceleration across both understanding and generation tasks while maintaining SOTA performance, outperforming competing unified models and validating our task-aware acceleration paradigm. Our code is publicly available at <https://github.com/Rirayh/FlashU>.

*Equal Contribution.

†Corresponding author: zhanglinfeng@sjtu.edu.cn

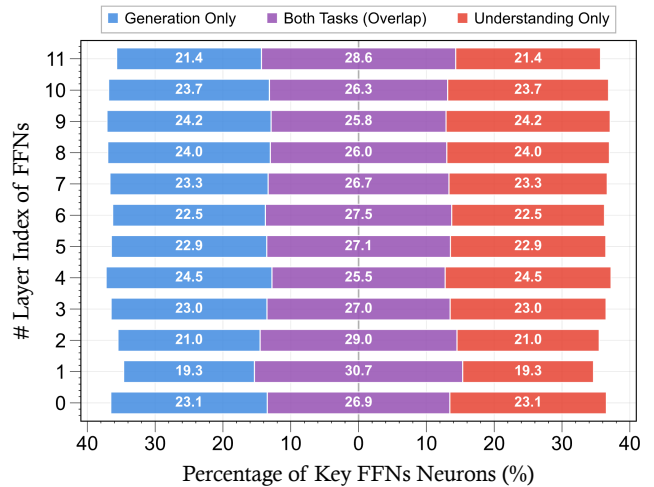


Figure 1. **Task-specific FFN neuron analysis for generation and understanding.** Each layer shows the fraction of neurons that are specific to generation, understanding, or shared between both tasks (excluding unimportant neurons). Percentages indicate the proportion of neurons in each layer ranked among the top 50% for task importance, as measured by OBD-inspired sensitivity scores Δ_i .

1. Introduction

With the rapid development of multi-modal large language models [1, 31, 55, 56, 66–68, 79, 81] and image generation models [10, 27, 28, 30, 49], researchers increasingly focus on integrating multimodal understanding and generation capabilities into a single model [82]. The emergence of unified models has marked a paradigm shift in multimodal AI, breaking down the traditional boundaries between understanding and generative tasks within a single architecture [74]. However, this versatility comes at the cost of substantial computational overhead. As model parameters continue to scale, achieving efficient inference acceleration has emerged as a pivotal challenge in translating these models from research to real-world deployment [67].

While significant strides have been made in model ac-

celeration techniques [4, 9, 22, 36, 39, 40, 51, 63–65, 75], systematic investigation into redundancy analysis and efficiency optimization for unified models remain largely unexplored. Existing acceleration methods, such as structured pruning [45] or quantization [37], typically adopt a *static and monolithic* strategy, which rests upon an untested assumption that the model’s computational requirements are homogeneous across all tasks. We contend that this assumption overlooks a fundamental contradiction within unified models: the intrinsic computational profiles of iterative generation tasks (e.g., diffusion processes) [77] and single-pass understanding tasks (e.g., VQA) [41] are fundamentally distinct. Generation tasks resemble solving ordinary differential equations (ODEs) [42], representing a multi-step denoising process that evolves from blurry to clear, where early steps exhibit high fault tolerance. Conversely, understanding tasks rely on the hierarchical abstraction and evolution of features within a single forward pass. Imposing a uniform acceleration strategy on unified models inevitably leads to a trade-off between competing objectives.

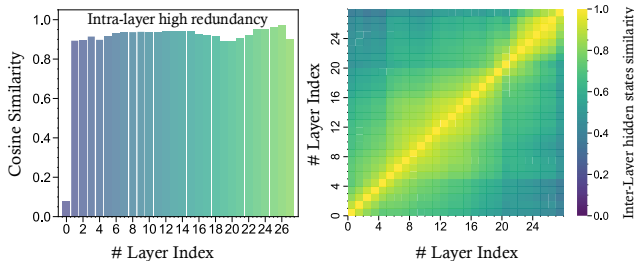


Figure 2. **Understanding Redundancy.** **Left:** Intra-layer cosine similarity between the input and output features of each layer for newly generated tokens in understanding tasks. **Right:** Inter-layer heatmap of the cosine similarity among layer outputs for newly generated tokens. All measurements were conducted on samples from the MME [19].

To bridge this gap, we present the first systematic dissection of the internal computational mechanisms of unified models, revealing two pivotal phenomena. First, we observe pronounced parameter specialization: the model’s feed-forward networks (FFNs) contain numerous neurons exclusively important for either generation or understanding tasks, with only a limited proportion of shared critical neurons (Figure 1). This indicates that despite a unified architecture, the model spontaneously develops task-specific computational pathways internally. Second, inter-layer similarity analysis reveals that generation tasks exhibit exceptionally high feature redundancy across layers during the denoising process, while key tokens in understanding tasks demonstrate progressively evolving features with increasing depth, rendering them more sensitive to intermediate layer pruning (Figure 2).

These findings compellingly demonstrate that for unified models, an “optimal” acceleration strategy must be task-

aware and dynamic.

Building upon this insight, we introduce **FlashU**, a training-free and task-aware acceleration framework for unified generative-understanding models. Our core principle is that acceleration strategies should align with, rather than oppose, the model’s internal parameter specialization mechanisms. For generation tasks, we conceptualize the process as a *coarse-to-fine* optimization problem, designing a Hybrid FFN that dynamically switches between lightweight and full paths during different generation phases, coupled with an adaptive ODE solver featuring multi-stage guidance and iterative caching. For understanding tasks, we combine static pruning of generation-exclusive neurons with dynamic visual token pruning to eliminate spatial redundancy. The distinguishing characteristic of our framework is its orthogonality: static pruning in understanding tasks preserves generative capacity while coexisting seamlessly with dynamic pathways in generation tasks through shared-weight design. In summary, our contributions are threefold:

- We conduct the first systematic investigation of internal computational redundancy in unified generative-understanding models, revealing the phenomena of parameter specialization and computational heterogeneity.
- We introduce the first training-free and task-aware acceleration framework for native unified models, enabling adaptive acceleration that aligns with the model’s internal inference pathways.
- Extensive experiments on Show-o2 demonstrate that our framework achieves $1.78\times$ to $2.01\times$ inference acceleration across both understanding and generation tasks while maintaining SOTA performance, outperforming competing unified models.

2. Related Work

Multimodal Large Language Models. Building on the significant progress of Large Language Models (LLMs) [59, 76], Multimodal Large Language Models (MLLMs) [1, 11, 38] have demonstrated remarkable capabilities in general-purpose visual understanding and reasoning. The predominant architecture utilizes a pre-trained vision encoder to extract visual features, which are subsequently projected and aligned with the LLM’s embedding space. Concurrently, a subset of MLLMs, known as encoder-free models [15, 16, 71], has emerged, aiming to directly align raw visual features within this space. However, these methods typically trail in performance compared to their counterparts that use aligned image-text features. Beyond architectural considerations, recent research [6, 31, 57] has emphasized the critical role of high-quality, large-scale instruction-tuning data in advancing MLLM capabilities.

Unified Multimodal Models. Unified Multimodal Mod-

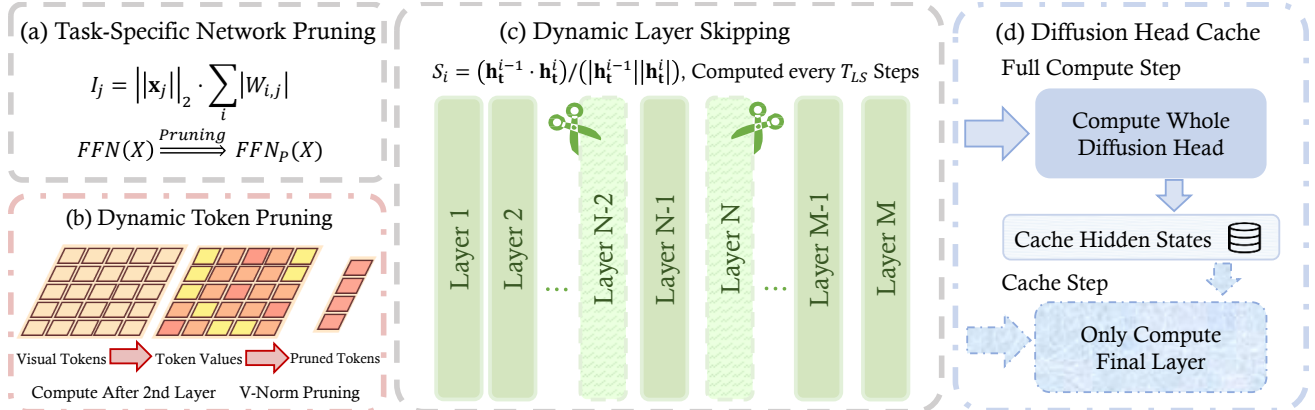


Figure 3. **Illustration of the FlashU acceleration framework.** (a) **Task-Specific FFN Pruning** calculates an importance score I_j based on activation norms and weight magnitude to statically mask redundant neurons for a specific task. (b) **Dynamic Token Pruning** utilizes the V-Norm proxy at shallow layers (the 2nd layer) to identify and prune visually spatially redundant tokens. (c) **Dynamic Layer Skipping** bypasses layers exhibiting high input-output cosine similarity (S_i), re-evaluating the skipping mask every T_{LS} steps. (d) **Diffusion Head Cache** exploits temporal coherence in the generative process, computing the full diffusion head only at fixed intervals and reusing cached hidden states for intermediate steps.

els (UMMs) represent an emerging research area focused on integrating the distinct capabilities of Large Multimodal Models (LMMs) and visual generative models into a single, cohesive system. This field has primarily advanced along two paradigms. The first approach involves developing native unified models [54, 62, 70, 71, 83], which feature a unified architecture inherently designed for both multimodal understanding and generation, often employing autoregressive modeling, diffusion, or a hybrid of these techniques. Subsequent research in this area has focused on refining training pipelines and enhancing the semantic richness of discrete visual tokens [12, 25, 44, 50]. The second paradigm involves assembling specialized, off-the-shelf components [5, 17, 20, 43, 47, 53, 58]. This method connects pre-trained LMMs for understanding with visual generative models for generation, typically by fine-tuning lightweight adapters or learnable query tokens. Representative works [5, 20, 47] have demonstrated the significant capabilities of these assembled frameworks, underscoring their potential as an efficient pathway toward unification.

3. Methodology

3.1. Overview

Our approach is founded on the principle of aligning optimization with the model’s intrinsic parameter specialization, wherein distinct neural circuits are dedicated to either generation or understanding tasks.

We first implement network redundancy elimination. A unified Feed-Forward Network (FFN) pruning policy accelerates both generation and understanding, while retaining the original FFNs to form a Hybrid FFN. Furthermore, we

introduce Dynamic Layer Skipping. This strategy specifically targets and eliminates inter-layer redundancy, thereby augmenting the redundancy elimination achieved by the preceding FFN method.

Beyond these foundational redundancy elimination, FlashU establishes two orthogonal, non-interfering acceleration paths within the single model, rather than imposing a uniform optimization. This dual-mode architecture allows the model to dynamically select the most efficient computational graph based on the task’s unique demands.

For iterative generative tasks, the framework employs an adaptive ODE solver augmented with dynamic guidance scaling and diffusion head iterative caching.

For single-pass understanding tasks, it utilizes visual token pruning in addition to the aforementioned network redundancy elimination techniques, which effectively mitigates spatial and computational redundancy.

3.2. Motivation

3.2.1. Parameter Specialization

Our investigation begins with a fundamental question: *do unified models utilize their parameters monolithically across different tasks?* Traditional acceleration methods implicitly assume so, applying a uniform optimization strategy. We challenge this assumption by analyzing the phenomenon of parameter specialization.

To quantify the task-specific importance of individual neurons, we employ a sensitivity analysis method inspired by Optimal Brain Damage (OBD). While traditional OBD assesses parameter saliency based on the global loss, we adapt this concept to evaluate a neuron’s contribution to the layer’s local output. For each neuron i in an FFN, we com-

pute an importance score Δ_i as the reconstruction error incurred by zeroing out that neuron’s activation:

$$\Delta_i = \mathbb{E}_{x \sim \mathcal{D}} \left[\|\text{FFN}(x) - \text{FFN}_{-i}(x)\|_2^2 \right] \quad (1)$$

where \mathcal{D} is a calibration dataset, $\text{FFN}(x)$ is the layer’s original output, and $\text{FFN}_{-i}(x)$ is its output with neuron i zeroed out. This directly measures the expected local feature degradation if that neuron were to be removed. We compute two separate scores for each neuron: a generation score Δ_i^G using a subset of the text-to-image generation dataset (DPG-Bench [23]), and an understanding score Δ_i^U using a subset of the VQA dataset (MME [19]).

Our analysis reveals a pronounced pattern of parameter specialization within the FFNs in both generation and understanding tasks. We observe that a significant portion of neurons are exclusively critical for either generation (high Δ_i^G , low Δ_i^U) or understanding (low Δ_i^G , high Δ_i^U). As shown in Figure 1, only a small subset of neurons are important for both tasks, confirming that the model forms distinct pathways internally. This insight motivates our framework: effective acceleration should leverage such specialization by designing dedicated optimization paths aligned with task-specific structures.

3.2.2. Temporal Redundancy

While the unified model operates in distinct modes (full self-attention for generation and causal self-attention for understanding), our analysis reveals a common opportunity for optimization. As illustrated in Figure 4 and Figure 2, we observe great inter-layer redundancy in both tasks by visualizing the similarity between layer inputs and outputs.

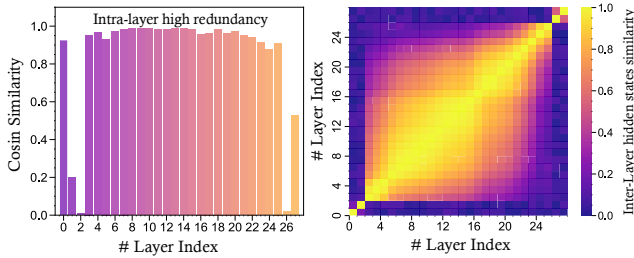


Figure 4. **Redundancy in Generation Tasks.** **Left:** Intra-layer cosine similarity between the input and output of each layer. **Right:** Inter-layer heatmap of hidden state cosine similarity. All measurements were conducted on samples from the GenEval [21].

3.3. Task-Specific Network Pruning

Our network pruning methodology is bifurcated into two complementary strategies: Task-Specific FFN Pruning and Dynamic Layer Skipping. The former addresses intra-layer redundancy by applying a one-shot, task-aware pruning mask to FFNs, while preserving the vanilla weights for hybrid computation. The latter addresses inter-layer redundancy by dynamically bypassing layers based on an input-output similarity metric, which is re-evaluated at intervals.

3.3.1. Task-Specific FFN Pruning

Our design for generation acceleration is motivated by the observation that parameters within the unified model exhibit a high degree of task specialization. As illustrated in Figure 1, distinct sets of neurons are critical exclusively for either generation or understanding tasks. This specialization implies that when executing a given task, the full computational power of the FFN layers is not required, as a substantial portion of the parameters may be non-essential. To balance computational cost and quality, we introduce a **Hybrid FFN** architecture. This architecture consists of both a *full path* (FFN_f) and a *pruned path* (FFN_p), allowing the model to alternate between them based on the timestep t .

Inspired by Wanda [52], we compute an importance score I_j for each neuron j . This score is the product of the component’s aggregate weight magnitude and its corresponding mean input activation norm:

$$I_j = \|\mathbf{x}_j\|_2 \cdot \sum_i |W_{i,j}|. \quad (2)$$

The activation norms $\|\mathbf{x}_j\|_2$ are gathered empirically: For image generation tasks, we collect these statistics during the generation process of the first image; For understanding tasks, we compute the norms at initialization using a 20-sample subset of the MME dataset.

This score I_j is used to create a static mask \mathbf{M} that defines the pruned path FFN_p . We prune the r_p proportion of FFN hidden dimension parameters, corresponding to the neurons with the lowest r_p ratio of I_j scores. The operation is defined as:

$$\text{FFN}_p(x) = W_2(\mathbf{M} \odot \sigma(W_1x + b_1)) + b_2. \quad (3)$$

where σ is the activation function and \odot denotes element-wise multiplication. The final output of the Hybrid FFN is formulated using an indicator function $\mathbf{1}(\cdot)$ based on a switching threshold τ (defaulting to 0.2):

$$y_h(x, t) = \mathbf{1}(t \leq \tau T) \cdot \text{FFN}_f(x) + \mathbf{1}(t > \tau T) \cdot \text{FFN}_p(x). \quad (4)$$

This significantly reduces the expected computational cost $\mathbb{E}[C]$ over the total duration T :

$$\mathbb{E}[C] = \tau C_f + (1 - \tau)C_p. \quad (5)$$

3.3.2. Dynamic Layer Skipping

To address the inter-layer redundancy illustrated in Figure 4 and Figure 2, we designed the **Dynamic Layer Skipping** strategy, which dynamically identifies and bypasses redundant layers within fixed intervals. A layer’s contribution is quantified by measuring its functional transformation. We define a similarity score S_i for each layer i , computed via cosine similarity between its input and output. For **generation tasks**, which update the entire sequence via full self-attention, we compute the mean cosine similarity between

a layer’s input hidden state \mathbf{H}_i and its output hidden state \mathbf{H}_{i+1} across a batch D :

$$S_i^{\text{gen}} = \frac{1}{D} \sum_{d=1}^D \frac{\mathbf{H}_i^{(d)} \cdot \mathbf{H}_{i+1}^{(d)}}{\|\mathbf{H}_i^{(d)}\|_2 \cdot \|\mathbf{H}_{i+1}^{(d)}\|_2} \quad (6)$$

A similarity score S_i^{gen} approaching 1 signifies high redundancy, as the layer’s output vector is directionally similar to its input, implying a minimal transformation. Conversely, for **understanding tasks**, which employ causal self-attention, computation is focused on the newly generated token. We therefore measure similarity by considering only the transformation of the hidden state at the final token position, \mathbf{h}_{t_L} . The score is computed across the batch D :

$$S_i^{\text{und}} = \frac{1}{D} \sum_{d=1}^D \frac{\mathbf{h}_{i,t_L}^{(d)} \cdot \mathbf{h}_{i+1,t_L}^{(d)}}{\|\mathbf{h}_{i,t_L}^{(d)}\|_2 \cdot \|\mathbf{h}_{i+1,t_L}^{(d)}\|_2} \quad (7)$$

The skipping policy is applied dynamically and updated periodically. We define a recalculation interval, T_{LS} . In the full-computation step of each interval, the model executes a forward pass using all layers. This step is leveraged to re-compute the similarity score S_i for every layer, leading to the generation of a new skip list, $\mathcal{L}_{\text{skip}}$. This list contains the indices of the layers with the highest similarity scores (i.e., the most redundant layers) determined by a predefined skipping ratio r_{LS} . The derived skip list $\mathcal{L}_{\text{skip}}$ is cached and subsequently applied for the duration of the following $T_{LS} - 1$ steps, enabling the model’s forward pass to bypass the full computation for any layer $i \in \mathcal{L}_{\text{skip}}$.

3.4. Generation Acceleration

The acceleration for iterative denoising generation tasks is designed around a coarse-to-fine optimization principle, viewing the process as the numerical solution to an Ordinary Differential Equation (ODE). Our approach introduces two synergistic optimizations that enhance this numerical solution: time-varying control signal for guidance scale and a temporal approximation for diffusion head via diffusion head cache.

3.4.1. Adaptive Guidance Scale

Standard approaches employ a static, high guidance scale s , a known trade-off that often introduces over-saturation or requires a high Number of Function Evaluations (NFE) to converge. The design of $s(t)$ is critical and non-trivial. Recent work [26] has established that the diffusion process is stage-wise, beginning with a “Mode Selection” phase (high t , high noise) and concluding with a “Concentration” phase (low t , low noise). A key finding is that strong, early guidance can be detrimental, as it “erodes global diversity” [26] by forcing a premature collapse during the Mode Selection phase. Based on this understanding, we propose a principled, ascending guidance schedule $s(t)$ that begins with a

low-gain regime and transitions to a high-gain regime:

$$s(t) = s_{\text{low}} \cdot \mathbf{1}(t > t_{\text{switch}}) + s_{\text{high}} \cdot \mathbf{1}(t \leq t_{\text{switch}}). \quad (8)$$

This strategy is strongly supported. Our use of low-gain control (s_{low}) during the early, high-noise stage ($t > t_{\text{switch}}$) respects the stochastic nature of the Mode Selection phase, preserving global diversity [26] while preventing the “overshooting” artifacts associated with static guidance [61]. The subsequent switch to high-gain control (s_{high}) during the late-stage ($t \leq t_{\text{switch}}$) effectively amplifies within-mode contraction, aligning with the “Concentration” phase to refine fidelity. This dynamic, monotonically increasing schedule, which [61] empirically demonstrates improves performance—is not just a qualitative improvement; it is a key enabler for acceleration. By increasing the guidance efficacy in the final steps, it allows the model to achieve high fidelity with significantly fewer total steps. Furthermore, this strategy creates a powerful computational synergy.

3.4.2. Diffusion Head Cache

The Diffusion Head component, responsible for predicting the velocity \hat{v}_θ of the denoising flow, often contains a series of computationally intensive layers. To mitigate this overhead, we introduce the Diffusion Head Cache, a mechanism designed to leverage the inherent temporal coherence observed across successive diffusion steps by periodically reusing expensive computations.

The flow dynamically selects one of two operational pathways at each timestep t based on a predefined cache interval, $\mathcal{T}_{\text{cache}}$. When the current step number is a multiple of the cache interval, the model executes the standard, full computation and cache the hidden state before the last layer. In all other subsequent steps (i.e., $t \pmod{\mathcal{T}_{\text{cache}}} \neq 0$), the model bypasses the costly Diffusion Head layers entirely. Instead, the required processed hidden state is read directly from the cache, effectively utilizing the result computed during the last full-computation step. This temporal approximation significantly reduces inference latency.

3.5. Understanding Acceleration

3.5.1. Dynamic Token Pruning via V-Norm Proxy

Building upon the pruned model, we introduce a dynamic mechanism to exploit the spatial redundancy of visual inputs. While prevailing token pruning methods rely on attention scores [8], this approach is incompatible with modern, optimized implementations like Flash Attention [13, 14], which avoid materializing the full attention matrix. Our solution is an efficient proxy for token importance. We empirically observe a consistent negative correlation between a token’s attention score and the L2 norm of its value vector (v-norm), as shown in Figure 5. This indicates that tokens with high attention scores (i.e., high importance) tend to have smaller v-norms.

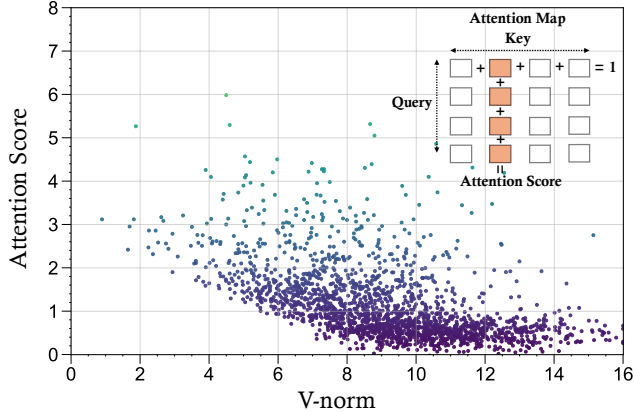


Figure 5. The relation between attention score and the norm of the value matrix for each token. Tokens with the largest attention score tend to have a lower norm in the value matrix.

Leveraging this insight, we use the v-norm as a low-cost, Flash Attention-compatible proxy for visual token pruning. In a shallow layer (e.g., the second layer), we compute the importance score I_j for each visual token \mathbf{t}_j as the L2 norm of its value vector \mathbf{v}_j : $I_j = \|\mathbf{v}_j\|_2$. We then prune a predefined ratio ρ of the tokens with the highest v-norm scores.

4. Experiments

4.1. Experimental Setup

Baselines and Benchmarks. To evaluate our method, we compare it against a diverse set of state-of-the-art (SOTA) models. Our primary latency-performance comparison is conducted against native unified models that share architectural similarities with our work, namely VILA-U [70], Show-o2 [72], and Emu3 [62]. For a more comprehensive assessment, we expand our comparison to include a broader range of advanced systems. This includes other unified models such as MetaMorph [58], ILLUME [60], JanusFlow [46], SynerGen-VL [33], Liquid [69], SEED-X [20], and Transfusion [83], as well as leading text-to-image generation models like D-DiT [34], Hunyuan-DiT [35], Playground v2.5 [32], PixArt- Σ [3], DALL-E 3 [2], SD3-Medium [18], TokenFlow-XL* [48], and MUSE-VL [73]. For evaluation, we assess multimodal understanding on a suite of benchmarks including MME [19], GQA [24], MMBench [41], MMMU [78], MMStar [7], and AI2D [29]. Visual generation capabilities are evaluated using the GenEval [21] and DPG-Bench [23], with detailed results presented in Tables 2 and 3. For more details on baselines and benchmarks, please refer to Appendix.

Implementation Details. Our method is primarily validated on the Show-o2 framework [72]. All experiments are conducted using PyTorch on NVIDIA A100-80GB GPUs. Multimodal understanding capabilities are evaluated via the Imms-eval [80], while generation performance is assessed following the protocols of GenEval and DPG-Bench.

4.2. Experimental Results

We apply FlashU to the state-of-the-art native unified model, Show-o2 [72], to demonstrate its effectiveness across both 1.5B and 7B model scales. As shown in Tables 1, 2, and 3, our method achieves significant latency reduction while maintaining SOTA performance against models with equivalent or larger parameter counts.

Multi-modal Understanding. Table 1 presents the impact of FlashU on multimodal understanding benchmarks. The vanilla Show-o2 (7B) model achieves strong SOTA performance but incurs a latency of 1.71 seconds. Our proposed FlashU reduces this to 0.96 seconds, achieving a $1.78\times$ speedup with minimal performance trade-off. Meanwhile, the accelerated FlashU (7B) model maintains its SOTA status against all baselines while demonstrating superior performance-latency trade-offs. Specifically, FlashU (7B) outperforms the larger Emu3 (8B) model in both performance (75.3 vs. 58.5 on MMB) and inference speed (0.96s vs. 1.29s). While VILA-U (7B) achieves exceptionally low latency (0.12s), our accelerated model retains substantial performance advantages across all benchmarks (e.g., 45.1 vs. 30.7 on MMMU), validating FlashU as an effective solution for performance-aware deployment.

Image Generation. We evaluate FlashU on visual generation tasks using the GenEval (Table 2) and DPG-Bench (Table 3). Both benchmarks consistently demonstrate that FlashU provides substantial acceleration (approximately $1.9\times$ to $2.0\times$) while preserving the original model’s SOTA capabilities. On GenEval, FlashU achieves a $1.92\times$ speedup for the 7B model (22.74s to 11.82s) and a $2.01\times$ speedup for the 1.5B model (10.61s to 5.28s). The accelerated 7B model’s Overall score (0.72) remains superior to other unified baselines, including Emu3 (0.66) and VILA-U (0.47). On DPG-Bench, FlashU delivers a $1.92\times$ speedup for the 7B model (11.30s to 5.89s) and a $1.85\times$ speedup for the 1.5B model (5.23s to 2.82s). Despite this significant latency reduction, the accelerated 7B model’s Overall score of 84.39 remains highly competitive, surpassing SOTA generation-specific models like SD3-Medium (84.08) and decisively outperforming VILA-U (74.26).

Efficiency and Performance Summary. Across all tasks and model scales, FlashU consistently delivers inference acceleration ranging from $1.78\times$ to $2.01\times$ without compromising the original Show-o2 model’s SOTA status. Our accelerated framework maintains a clear performance lead over competing unified models while operating at a fraction of the computational cost, demonstrating an effective and practical solution for deploying large-scale unified models. Meanwhile, as shown in Figure 6, our accelerated framework produces generations that remain highly faithful to the prompt, even surpassing the vanilla model in instruction following and matching every specified detail.

Table 1. Evaluation on multimodal understanding benchmarks. # Params. indicates the number of parameters of the base LLM. Results in gray indicate the vanilla Show-o2 performance. Latency is measured in seconds (s), conducted on samples from MMMU.

Models	# Params.	MME ↑ (p)	GQA↑	MMB ↑ (en)	MMMU ↑ (val)	MMStar ↑	AI2D ↑	Latency (s) ↓
MetaMorph [58]	8B	-	-	75.2	-	-	-	-
ILLUME [60]	7B	1445.3	-	75.1	38.2	-	71.4	-
Show-o [71]	1.3B	1097.2	58.0	-	27.4	-	-	-
JanusFlow [46]	1.5B	1333.1	60.3	74.9	29.3	-	-	-
SynerGen-VL [33]	2.4B	1381.0	-	53.7	34.2	-	-	-
Liquid [69]	8B	1448.0	61.1	-	-	-	-	-
Emu3 [62]	8B	-	60.3	58.5	31.6	-	70.0	1.29
VILA-U [70]	7B	1317.4	58.5	63.5	30.7	37.2	48.9	0.12
Show-o2 [72]	1.5B	1450.9	60.0	67.4	37.1	43.4	69.0	-
Show-o2 [72]	7B	1620.5	63.1	79.3	48.9	56.6	78.6	1.71
+ FlashU (Ours)	7B	1560.5	60.4	75.3	45.1	48.3	73.3	0.96 _{+1.78×}

Table 2. Evaluation on the GenEval [21]. # Params. indicates the number of parameters of the base LLM. Results in gray indicate the vanilla Show-o2 performance. The subscript values show the speedup achieved by FlashU. Latency is measured in seconds (s).

Method	# Params.	Single Obj.	Two Obj.	Counting	Colors	Position	Color Attri.	Overall↑	Latency (s)↓
SEED-X [20]	17B	0.97	0.58	0.26	0.80	0.19	0.14	0.49	-
TokenFlow-XL [48]	14B	0.95	0.60	0.41	0.81	0.16	0.24	0.55	-
ILLUME [60]	7B	0.99	0.86	0.45	0.71	0.39	0.28	0.61	-
Show-o [71]	1.3B	0.98	0.80	0.66	0.84	0.31	0.50	0.68	-
MUSE-VL [73]	7B	-	-	-	-	-	-	0.57	-
Transfusion [83]	3.5B	-	-	-	-	-	-	0.63	-
D-DiT [34]	2B	0.97	0.80	0.54	0.76	0.32	0.50	0.65	-
Emu3 [62]	8B	-	-	-	-	-	-	0.66	110.5
VILA-U [70]	7B	0.89	0.62	0.36	0.79	0.20	0.23	0.47	13.58
Show-o2 [72]	1.5B	0.99	0.86	0.55	0.86	0.46	0.63	0.73	10.61
+ FlashU (Ours)	1.5B	0.99	0.84	0.54	0.85	0.41	0.61	0.71	5.28 _{+2.01×}
Show-o2 [72]	7B	1.00	0.87	0.58	0.92	0.52	0.62	0.76	22.74
+ FlashU (Ours)	7B	0.99	0.80	0.53	0.89	0.46	0.58	0.72	11.82 _{+1.92×}



A vibrant canvas stretched across a 2cm thick **wooden frame**, adorned with illustration of **abstract, beautiful female faces depicted on three separate segments** of canvas. The artwork displays a unique juxtaposition of blooming flowers and the delicate features of women, with a rich color palette that includes hues of **purple, red, and yellow**. Each of the **three portions of the canvas seamlessly connects**, creating a continuous visual narrative that celebrates feminine beauty and botanical elegance.



☹️ Emu3-DPO 8B

- ! three separate segments
- ! three portions of the canvas seamlessly connects

120.1 seconds



☹️ VILA-U 7B

- ! three separate segments
- ! three portions of the canvas seamlessly connects

7.83 seconds



☹️ Show o2 1.5B

- 🌀 three separate segments
- ! three portions of the canvas seamlessly connects

6.15 seconds



😊 FlashU 1.5B (Ours)

- 🌀 three separate segments
- 🌀 three portions of the canvas seamlessly connects

2.17 seconds

Figure 6. Comparison of four unified multimodal models on generating a three-panel canvas with seamless cross-panel continuity. While baseline models fail to satisfy the structural or continuity requirements, our FlashU 1.5B (from Show-o2 [72]) accurately produces all three aligned segments with the fastest inference time.

Table 3. Evaluation on DPG-Bench [23]. # Params. denotes the parameter count of the base LLM. Results in gray correspond to vanilla Show-o2. Subscripts indicate the speedup of FlashU. Latency is reported in seconds (s), averaged per sample.

Method	# Params.	Global	Entity	Attribute	Relation	Overall \uparrow	Latency (s) \downarrow
Hunyuan-DiT [35]	1.5B	84.59	80.59	88.01	74.36	78.87	-
Playground v2.5 [32]	-	83.06	82.59	81.20	84.08	75.47	-
PixArt- Σ [3]	-	86.89	82.89	88.94	86.59	80.54	-
DALL-E 3 [2]	-	90.97	89.61	88.39	90.58	83.50	-
SD3-Medium [18]	2B	87.90	91.01	88.83	80.70	84.08	-
Emu3-DPO [62]	8B	-	-	-	-	81.60	124.8
VILA-U [70]	7B	89.92	82.73	80.80	87.83	74.26	9.78
Show-o2 [72]	1.5B	87.53	90.38	91.34	90.30	85.02	5.23
+ FlashU (Ours)	1.5B	84.19	89.48	90.98	90.38	84.12	2.82 _{+1.85\times}
Show-o2 [72]	7B	89.00	91.78	89.96	91.81	86.14	11.30
+ FlashU (Ours)	7B	87.79	90.30	89.29	90.30	84.39	5.89 _{+1.92\times}

4.3. Ablation Study

To validate the individual contributions of our components, we conducted an ablation study on both the 7B and 1.5B models using the DPG-Bench [23] benchmark. Results are detailed in Tables 4 and 5 for the 7B and 1.5B models, respectively. We establish FFN pruning as the acceleration baseline, achieving an overall speedup of around 1.3 \times . Building upon this static pruning, our dynamic technologies account for the majority of the acceleration: Adaptive Guidance and Dynamic Layer Pruning jointly yield substantial additional speedup. The study also highlights the critical role of our Hybrid Network module. Disabling this module results in a significant score drop, demonstrating its essential quality-preserving function in restoring fidelity.

Table 4. Ablation study on the 7B model of Show-o2 using DPG-Bench [23]. The subscript values show the speedup relative to Show-o2 baseline. Latency is measured in seconds (s).

Strategy	Latency (s)	Score
Show-o2 [72]	11.30	86.14
FlashU (Ours)	5.89 _{+1.92\times}	84.39
<i>w/o Dynamic Layer Pruning</i>	6.70 _{+1.69\times}	85.56
<i>w/o Hybrid Network</i>	5.65 _{+2.00\times}	83.68
<i>w/o Adaptive Guidance</i>	8.86 _{+1.28\times}	85.34
<i>FFN Pruning Only</i>	9.21 _{+1.23\times}	85.08

5. Conclusion

We present a fundamental shift in accelerating unified multimodal models through systematic analysis revealing that these models, despite their monolithic architecture, inherently develop task-specific computational pathways. This discovery challenges conventional uniform acceleration strategies and establishes task-aware optimization that aligns with the model’s internal mechanisms. Our pro-

Table 5. Ablation study on the 1.5B model of Show-o2 using DPG-Bench [23]. The subscript values show the speedup relative to Show-o2 baseline. Latency is measured in seconds (s).

Strategy	Latency (s)	Score
Show-o2 [72]	5.23	85.02
FlashU (Ours)	2.80 _{+1.87\times}	84.12
<i>w/o Dynamic Layer Pruning</i>	2.91 _{+1.80\times}	85.33
<i>w/o Hybrid Network</i>	2.48 _{+2.11\times}	83.57
<i>w/o Adaptive Guidance</i>	3.92 _{+1.33\times}	83.42
<i>FFN Pruning Only</i>	3.84 _{+1.36\times}	84.27

posed **FlashU** demonstrates that respecting this natural specialization enables 1.78 \times to 2.01 \times speedup while maintaining SOTA performance across understanding and generation tasks. These results validate that unified models benefit from task-specific acceleration rather than one-size-fits-all approaches. As unified models continue to scale, task-aware acceleration grounded in deep understanding of model internals represents a promising direction for practical real-world deployment. Moreover, our analysis provides a unified lens for interpreting efficiency behaviors observed across diverse multimodal architectures. FlashU further highlights that efficient inference does not require sacrificing representational richness when model structure is properly leveraged. We believe this paradigm will inspire future research on principled, model-aligned acceleration methods for next generation of unified multimodal systems.

Acknowledgements

This work was supported by the Shanghai Science and Technology Program (Grant No. 25ZR1402278) and WUYING - Alibaba Cloud.

References

- [1] Shuai Bai, Keqin Chen, Xuejing Liu, Jialin Wang, Wenbin Ge, Sibao Song, Kai Dang, Peng Wang, Shijie Wang, Jun Tang, Humen Zhong, Yuanzhi Zhu, Mingkun Yang, Zhao-hai Li, Jianqiang Wan, Pengfei Wang, Wei Ding, Zheren Fu, Yiheng Xu, Jiabo Ye, Xi Zhang, Tianbao Xie, Zesen Cheng, Hang Zhang, Zhibo Yang, Haiyang Xu, and Junyang Lin. Qwen2.5-vl technical report. *arXiv preprint arXiv:2502.13923*, 2025. 1, 2
- [2] James Betker, Gabriel Goh, Li Jing, Tim Brooks, Jianfeng Wang, Linjie Li, Long Ouyang, Juntang Zhuang, Joyce Lee, Yufei Guo, et al. Improving image generation with better captions. *Computer Science*. <https://cdn.openai.com/papers/dall-e-3.pdf>, 2(3):8, 2023. 6, 8, 1
- [3] Junsong Chen, Chongjian Ge, Enze Xie, Yue Wu, Lewei Yao, Xiaozhe Ren, Zhongdao Wang, Ping Luo, Huchuan Lu, and Zhenguo Li. Pixart-sigma: Weak-to-strong training of diffusion transformer for 4k text-to-image generation, 2024. 6, 8, 1
- [4] Junjie Chen, Xuyang Liu, Zichen Wen, Yiyu Wang, Siteng Huang, and Honggang Chen. Variation-aware vision token dropping for faster large vision-language models. *arXiv preprint arXiv:2509.01552*, 2025. 2
- [5] Jiu-hai Chen, Zhiyang Xu, Xichen Pan, Yushi Hu, Can Qin, Tom Goldstein, Lifu Huang, Tianyi Zhou, Saining Xie, Silvio Savarese, et al. Blip3-o: A family of fully open unified multimodal models-architecture, training and dataset. *arXiv preprint arXiv:2505.09568*, 2025. 3
- [6] Lin Chen, Jisong Li, Xiaoyi Dong, Pan Zhang, Conghui He, Jiaqi Wang, Feng Zhao, and Dahua Lin. Sharegpt4v: Improving large multi-modal models with better captions. *arXiv preprint arXiv:2311.12793*, 2023. 2
- [7] Lin Chen, Jinsong Li, Xiaoyi Dong, Pan Zhang, Yuhang Zang, Zehui Chen, Haodong Duan, Jiaqi Wang, Yu Qiao, Dahua Lin, et al. Are we on the right way for evaluating large vision-language models? *arXiv preprint arXiv:2403.20330*, 2024. 6, 1
- [8] Liang Chen, Haozhe Zhao, Tianyu Liu, Shuai Bai, Junyang Lin, Chang Zhou, and Baobao Chang. An image is worth 1/2 tokens after layer 2: Plug-and-play inference acceleration for large vision-language models. In *European Conference on Computer Vision*, pages 19–35. Springer, 2024. 5
- [9] Yuan Chen, Zichen Wen, Yuzhou Wu, Xuyang Liu, Shuang Chen, Junpeng Ma, Weijia Li, Conghui He, and Linfeng Zhang. Ipcv: Information-preserving compression for mllm visual encoders. *arXiv preprint arXiv:2512.18747*, 2025. 2
- [10] Zhaorun Chen, Yichao Du, et al. Mj-bench: Is your multimodal reward model really a good judge for text-to-image generation? *arXiv preprint arXiv:2407.04842*, 2024. 1
- [11] Zhe Chen, Weiyun Wang, Yue Cao, Yangzhou Liu, Zhangwei Gao, Erfei Cui, Jinguo Zhu, Shenglong Ye, Hao Tian, Zhaoyang Liu, et al. Expanding performance boundaries of open-source multimodal models with model, data, and test-time scaling. *arXiv preprint arXiv:2412.05271*, 2024. 2
- [12] Zisheng Chen, Chunwei Wang, Xiuwei Chen, Hang Xu, Jianhua Han, and Xiaodan Liang. Semhitok: A unified image tokenizer via semantic-guided hierarchical codebook for multimodal understanding and generation. *arXiv preprint arXiv:2503.06764*, 2025. 3
- [13] Tri Dao. FlashAttention-2: Faster attention with better parallelism and work partitioning. In *International Conference on Learning Representations (ICLR)*, 2024. 5
- [14] Tri Dao, Daniel Y. Fu, Stefano Ermon, Atri Rudra, and Christopher Ré. FlashAttention: Fast and memory-efficient exact attention with IO-awareness. In *Advances in Neural Information Processing Systems (NeurIPS)*, 2022. 5
- [15] Haiwen Diao, Yufeng Cui, Xiaotong Li, Yuezhe Wang, Huchuan Lu, and Xinlong Wang. Unveiling encoder-free vision-language models. *arXiv preprint arXiv:2406.11832*, 2024. 2
- [16] Haiwen Diao, Xiaotong Li, Yufeng Cui, Yuezhe Wang, Haoge Deng, Ting Pan, Wenxuan Wang, Huchuan Lu, and Xinlong Wang. Evev2: Improved baselines for encoder-free vision-language models. *arXiv preprint arXiv:2502.06788*, 2025. 2
- [17] Runpei Dong, Chunrui Han, Yuang Peng, Zekun Qi, Zheng Ge, Jinrong Yang, Liang Zhao, Jianjian Sun, Hongyu Zhou, Haoran Wei, Xiangwen Kong, Xiangyu Zhang, Kaisheng Ma, and Li Yi. DreamLLM: Synergistic multimodal comprehension and creation. In *ICLR*, 2024. 3
- [18] Patrick Esser, Sumith Kulal, Andreas Blattmann, Rahim Entezari, Jonas Müller, Harry Saini, Yam Levi, Dominik Lorenz, Axel Sauer, Frederic Boesel, et al. Scaling rectified flow transformers for high-resolution image synthesis. In *ICML*, 2024. 6, 8, 1
- [19] Chaoyou Fu, Peixian Chen, Yunhang Shen, Yulei Qin, Mengdan Zhang, Xu Lin, Zhenyu Qiu, Wei Lin, Jinrui Yang, Xiawu Zheng, Ke Li, Xing Sun, and Rongrong Ji. MME: A comprehensive evaluation benchmark for multimodal large language models. *CoRR*, abs/2306.13394, 2023. 2, 4, 6, 1
- [20] Yuying Ge, Sijie Zhao, Jinguo Zhu, Yixiao Ge, Kun Yi, Lin Song, Chen Li, Xiaohan Ding, and Ying Shan. Seed-x: Multimodal models with unified multi-granularity comprehension and generation. *arXiv preprint arXiv:2404.14396*, 2024. 3, 6, 7, 1
- [21] Dhruba Ghosh, Hannaneh Hajishirzi, and Ludwig Schmidt. Geneval: An object-focused framework for evaluating text-to-image alignment. In *NeurIPS*, 2023. 4, 6, 7, 1
- [22] Peize He, Zichen Wen, Yubo Wang, Yuxuan Wang, Xiaoqian Liu, Jiajie Huang, Zehui Lei, Zhuangcheng Gu, Xiangqi Jin, Jiabing Yang, et al. Audiomarathon: A comprehensive benchmark for long-context audio understanding and efficiency in audio llms. *arXiv preprint arXiv:2510.07293*, 2025. 2
- [23] Xiwei Hu, Rui Wang, Yixiao Fang, Bin Fu, Pei Cheng, and Gang Yu. Ella: Equip diffusion models with llm for enhanced semantic alignment, 2024. 4, 6, 8, 1, 2
- [24] Drew A. Hudson and Christopher D. Manning. GQA: A new dataset for real-world visual reasoning and compositional question answering. In *CVPR*, pages 6700–6709. Computer Vision Foundation / IEEE, 2019. 6, 1
- [25] Yang Jiao, Haibo Qiu, Zequn Jie, Shaoxiang Chen, Jingjing Chen, Lin Ma, and Yu-Gang Jiang. Unitoken: Harmonizing multimodal understanding and generation through unified visual encoding. *arXiv preprint arXiv:2504.04423*, 2025. 3

- [26] Cheng Jin, Qitan Shi, and Yuantao Gu. Stage-wise dynamics of classifier-free guidance in diffusion models. *arXiv preprint arXiv:2509.22007*, 2025. 5
- [27] Hengrui Kang, Zhuangcheng Gu, Zhiyuan Zhao, Zichen Wen, Bin Wang, Weijia Li, and Conghui He. Omnidoclayout: Towards diverse document layout generation via coarse-to-fine llm learning. *arXiv preprint arXiv:2510.26213*, 2025. 1
- [28] Hengrui Kang, Siwei Wen, et al. Legion: Learning to ground and explain for synthetic image detection. *arXiv preprint arXiv:2503.15264*, 2025. 1
- [29] Aniruddha Kembhavi, Mike Salvato, Eric Kolve, Minjoon Seo, Hannaneh Hajishirzi, and Ali Farhadi. A diagram is worth a dozen images. In *Computer Vision–ECCV 2016: 14th European Conference, Amsterdam, The Netherlands, October 11–14, 2016, Proceedings, Part IV 14*, pages 235–251. Springer, 2016. 6, 1
- [30] Black Forest Labs, Stephen Batifol, Andreas Blattmann, Frederic Boesel, Saksham Consul, Cyril Diagne, Tim Dockhorn, Jack English, Zion English, Patrick Esser, et al. Flux. 1 kontext: Flow matching for in-context image generation and editing in latent space. *arXiv preprint arXiv:2506.15742*, 2025. 1
- [31] Bo Li, Yuanhan Zhang, Dong Guo, Renrui Zhang, Feng Li, Hao Zhang, Kaichen Zhang, Peiyuan Zhang, Yanwei Li, Ziwei Liu, et al. Llava-onevision: Easy visual task transfer. *arXiv preprint arXiv:2408.03326*, 2024. 1, 2
- [32] Daiqing Li, Aleks Kamko, Ehsan Akhgari, Ali Sabet, Linmiao Xu, and Suhail Doshi. Playground v2.5: Three insights towards enhancing aesthetic quality in text-to-image generation. *ArXiv*, abs/2402.17245, 2024. 6, 8, 1, 2
- [33] Hao Li, Changyao Tian, Jie Shao, Xizhou Zhu, Zhaokai Wang, Jinguo Zhu, Wenhan Dou, Xiaogang Wang, Hongsheng Li, Lewei Lu, and Jifeng Dai. Synergen-vl: Towards synergistic image understanding and generation with vision experts and token folding. *arXiv preprint arXiv:2412.09604*, 2024. 6, 7, 1
- [34] Zijie Li, Henry Li, Yichun Shi, Amir Barati Farimani, Yuval Kluger, Linjie Yang, and Peng Wang. Dual diffusion for unified image generation and understanding. *arXiv preprint arXiv:2501.00289*, 2024. 6, 7, 1
- [35] Zhimin Li, Jianwei Zhang, Qin Lin, Jiangfeng Xiong, Yanxin Long, Xincheng Deng, Yingfang Zhang, Xingchao Liu, Minbin Huang, Zedong Xiao, Dayou Chen, Jiajun He, Jiahao Li, Wenyue Li, Chen Zhang, Rongwei Quan, Jianxiang Lu, Jiabin Huang, Xiaoyan Yuan, Xiaoxiao Zheng, Yixuan Li, Jihong Zhang, Chao Zhang, Meng Chen, Jie Liu, Zheng Fang, Weiyan Wang, Jinbao Xue, Yangyu Tao, Jianchen Zhu, Kai Liu, Sihuan Lin, Yifu Sun, Yun Li, Dongdong Wang, Mingtao Chen, Zhichao Hu, Xiao Xiao, Yan Chen, Yuhong Liu, Wei Liu, Di Wang, Yong Yang, Jie Jiang, and Qinglin Lu. Hunyuan-dit: A powerful multi-resolution diffusion transformer with fine-grained chinese understanding, 2024. 6, 8, 1, 2
- [36] Chenfei Liao, Wensong Wang, Zichen Wen, Xu Zheng, Yiyu Wang, Haocong He, Yuanhuiyi Lyu, Lutao Jiang, Xin Zou, Yuqian Fu, et al. Are we using the right benchmark: An evaluation framework for visual token compression methods. *arXiv preprint arXiv:2510.07143*, 2025. 2
- [37] Ji Lin, Jiaming Tang, Haotian Tang, Shang Yang, Wei-Ming Chen, Wei-Chen Wang, Guangxuan Xiao, Xingyu Dang, Chuang Gan, and Song Han. Awq: Activation-aware weight quantization for on-device llm compression and acceleration. *Proceedings of machine learning and systems*, 6:87–100, 2024. 2
- [38] Haotian Liu, Chunyuan Li, Qingyang Wu, and Yong Jae Lee. Visual instruction tuning. *NeurIPS*, 36, 2024. 2
- [39] Xuyang Liu, Ziming Wang, Junjie Chen, Yuhang Han, Yingyao Wang, Jiale Yuan, Jun Song, Siteng Huang, and Honggang Chen. Global compression commander: Plug-and-play inference acceleration for high-resolution large vision-language models. *arXiv preprint arXiv:2501.05179*, 2025. 2
- [40] Xuyang Liu, Zichen Wen, Shaobo Wang, Junjie Chen, Zhishan Tao, Yubo Wang, Xiangqi Jin, Chang Zou, Yiyu Wang, Chenfei Liao, et al. Shifting ai efficiency from model-centric to data-centric compression. *arXiv preprint arXiv:2505.19147*, 2025. 2
- [41] Yuan Liu, Haodong Duan, Yuanhan Zhang, Bo Li, Songyang Zhang, Wangbo Zhao, Yike Yuan, Jiaqi Wang, Conghui He, Ziwei Liu, et al. Mmbench: Is your multi-modal model an all-around player? In *European conference on computer vision*, pages 216–233. Springer, 2024. 2, 6, 1
- [42] Cheng Lu, Yuhao Zhou, Fan Bao, Jianfei Chen, Chongxuan Li, and Jun Zhu. Dpm-solver: A fast ode solver for diffusion probabilistic model sampling in around 10 steps. *Advances in neural information processing systems*, 35:5775–5787, 2022. 2
- [43] Jiasen Lu, Christopher Clark, Sangho Lee, Zichen Zhang, Savya Khosla, Ryan Marten, Derek Hoiem, and Aniruddha Kembhavi. Unified-io 2: Scaling autoregressive multimodal models with vision, language, audio, and action. *arXiv preprint arXiv:2312.17172*, 2023. 3
- [44] Chuofan Ma, Yi Jiang, Junfeng Wu, Jihan Yang, Xin Yu, Zehuan Yuan, Bingyue Peng, and Xiaojuan Qi. Unitok: A unified tokenizer for visual generation and understanding. *arXiv preprint arXiv:2502.20321*, 2025. 3
- [45] Xinyin Ma, Gongfan Fang, and Xinchao Wang. Llm-pruner: On the structural pruning of large language models. *Advances in neural information processing systems*, 36:21702–21720, 2023. 2
- [46] Yiyang Ma, Xingchao Liu, Xiaokang Chen, Wen Liu, Chengyue Wu, Zhiyu Wu, Zizheng Pan, Zhenda Xie, Haowei Zhang, Xingkai yu, Liang Zhao, Yisong Wang, Jiaying Liu, and Chong Ruan. Janusflow: Harmonizing autoregression and rectified flow for unified multimodal understanding and generation, 2024. 6, 7, 1, 2
- [47] Xichen Pan, Satya Narayan Shukla, Aashu Singh, Zhuokai Zhao, Shlok Kumar Mishra, Jialiang Wang, Zhiyang Xu, Jihuai Chen, Kunpeng Li, Felix Juefei-Xu, Ji Hou, and Saining Xie. Transfer between modalities with metaqueries. *arXiv preprint arXiv:2504.06256*, 2025. 3
- [48] Liao Qu, Huichao Zhang, Yiheng Liu, Xu Wang, Yi Jiang, Yiming Gao, Hu Ye, Daniel K Du, Zehuan Yuan, and

- Xinglong Wu. Tokenflow: Unified image tokenizer for multimodal understanding and generation. *arXiv preprint arXiv:2412.03069*, 2024. 6, 7, 1, 2
- [49] Robin Rombach, Andreas Blattmann, Dominik Lorenz, Patrick Esser, and Björn Ommer. High-resolution image synthesis with latent diffusion models. In *CVPR*, pages 10684–10695, 2022. 1
- [50] Wei Song, Yuran Wang, Zijia Song, Yadong Li, Haoze Sun, Weipeng Chen, Zenan Zhou, Jianhua Xu, Jiaqi Wang, and Kaicheng Yu. Dualtoken: Towards unifying visual understanding and generation with dual visual vocabularies. *arXiv preprint arXiv:2503.14324*, 2025. 3
- [51] Sharath Turuvekere Sreenivas, Saurav Muralidharan, Raviraj Joshi, Marcin Chochowski, Ameya Sunil Mahabaleshwar, Gerald Shen, Jiaqi Zeng, Zijia Chen, Yoshi Suhara, Shizhe Diao, et al. Llm pruning and distillation in practice: The minitron approach. *arXiv preprint arXiv:2408.11796*, 2024. 2
- [52] Mingjie Sun, Zhuang Liu, Anna Bair, and J Zico Kolter. A simple and effective pruning approach for large language models. *arXiv preprint arXiv:2306.11695*, 2023. 4
- [53] Zineng Tang, Ziyi Yang, Chenguang Zhu, Michael Zeng, and Mohit Bansal. Any-to-any generation via composable diffusion. *NeurIPS*, 36, 2024. 3
- [54] Chameleon Team. Chameleon: Mixed-modal early-fusion foundation models. *arXiv preprint arXiv:2405.09818*, 2024. 3
- [55] Kimi Team, Angang Du, Bohong Yin, Bowei Xing, Bowen Qu, Bowen Wang, Cheng Chen, Chenlin Zhang, Chen-zhuang Du, Chu Wei, et al. Kimi-vl technical report. *arXiv preprint arXiv:2504.07491*, 2025. 1
- [56] Kimi Team, Tongtong Bai, Yifan Bai, Yiping Bao, SH Cai, Yuan Cao, Y Charles, HS Che, Cheng Chen, Guanduo Chen, et al. Kimi k2. 5: Visual agentic intelligence. *arXiv preprint arXiv:2602.02276*, 2026. 1
- [57] Shengbang Tong, Ellis Brown, Penghao Wu, Sanghyun Woo, Manoj Midepogu, Sai Charitha Akula, Jihan Yang, Shusheng Yang, Adithya Iyer, Xichen Pan, Austin Wang, Rob Fergus, Yann LeCun, and Saining Xie. Cambrian-1: A fully open, vision-centric exploration of multimodal llms, 2024. 2
- [58] Shengbang Tong, David Fan, Jiachen Zhu, Yunyang Xiong, Xinlei Chen, Koustuv Sinha, Michael Rabbat, Yann LeCun, Saining Xie, and Zhuang Liu. Metamorph: Multimodal understanding and generation via instruction tuning. *arXiv preprint arXiv:2412.14164*, 2024. 3, 6, 7, 1
- [59] Hugo Touvron, Thibaut Lavril, Gautier Izacard, Xavier Martinet, Marie-Anne Lachaux, Timothée Lacroix, Baptiste Rozière, Naman Goyal, Eric Hambro, Faisal Azhar, Aurélien Rodriguez, Armand Joulin, Edouard Grave, and Guillaume Lample. Llama: Open and efficient foundation language models. *CoRR*, abs/2302.13971, 2023. 2
- [60] Chunwei Wang, Guansong Lu, Junwei Yang, Runhui Huang, Jianhua Han, Lu Hou, Wei Zhang, and Hang Xu. ILLUME: illuminating your llms to see, draw, and self-enhance. *arXiv preprint arXiv:2412.06673*, 2024. 6, 7, 1
- [61] Xi Wang, Nicolas Dufour, Nefeli Andreou, Marie-Paule Cani, Victoria Fernández Abrevaya, David Picard, and Vicky Kalogeiton. Analysis of classifier-free guidance weight schedulers. *arXiv preprint arXiv:2404.13040*, 2024. 5
- [62] Xinlong Wang, Xiaosong Zhang, Zhengxiong Luo, Quan Sun, Yufeng Cui, Jinsheng Wang, Fan Zhang, Yueze Wang, Zhen Li, Qiyang Yu, et al. Emu3: Next-token prediction is all you need. *arXiv preprint arXiv:2409.18869*, 2024. 3, 6, 7, 8, 1, 2
- [63] Zichen Wen, Yifeng Gao, Weijia Li, Conghui He, and Linfeng Zhang. Token pruning in multimodal large language models: Are we solving the right problem? *arXiv preprint arXiv:2502.11501*, 2025. 2
- [64] Zichen Wen, Yifeng Gao, Shaobo Wang, Junyuan Zhang, Qintong Zhang, Weijia Li, Conghui He, and Linfeng Zhang. Stop looking for important tokens in multimodal language models: Duplication matters more. *arXiv preprint arXiv:2502.11494*, 2025.
- [65] Zichen Wen, Jiashu Qu, Zhaorun Chen, Xiaoya Lu, Dongrui Liu, Zhiyuan Liu, Ruixi Wu, Yicun Yang, Xiangqi Jin, Haoyun Xu, et al. The devil behind the mask: An emergent safety vulnerability of diffusion llms. *arXiv preprint arXiv:2507.11097*, 2025. 2
- [66] Zichen Wen, Shaobo Wang, Yufa Zhou, Junyuan Zhang, Qintong Zhang, Yifeng Gao, Zhaorun Chen, Bin Wang, Weijia Li, Conghui He, et al. Efficient multi-modal large language models via progressive consistency distillation. *arXiv preprint arXiv:2510.00515*, 2025. 1
- [67] Zichen Wen, Yiyu Wang, Chenfei Liao, Boxue Yang, Junxian Li, Weifeng Liu, Haocong He, Bolong Feng, Xuyang Liu, Yuanhuiyi Lyu, et al. Ai for service: Proactive assistance with ai glasses. *arXiv preprint arXiv:2510.14359*, 2025. 1
- [68] Zichen Wen, Boxue Yang, Shuang Chen, Yaojie Zhang, Yuhang Han, Junlong Ke, Cong Wang, Yicheng Fu, Jiawang Zhao, Jiangchao Yao, et al. Innovator-vl: A multimodal large language model for scientific discovery. *arXiv preprint arXiv:2601.19325*, 2026. 1
- [69] Junfeng Wu, Yi Jiang, Chuofan Ma, Yuliang Liu, Hengshuang Zhao, Zehuan Yuan, Song Bai, and Xiang Bai. Liquid: Language models are scalable multi-modal generators. *arXiv preprint arXiv:2412.04332*, 2024. 6, 7, 1, 2
- [70] Yecheng Wu, Zhuoyang Zhang, Junyu Chen, Haotian Tang, Dacheng Li, Yunhao Fang, Ligeng Zhu, Enze Xie, Hongxu Yin, Li Yi, et al. Vila-u: a unified foundation model integrating visual understanding and generation. *arXiv preprint arXiv:2409.04429*, 2024. 3, 6, 7, 8, 1, 2
- [71] Jinheng Xie, Weijia Mao, Zechen Bai, David Junhao Zhang, Weihao Wang, Kevin Qinghong Lin, Yuchao Gu, Zhijie Chen, Zhenheng Yang, and Mike Zheng Shou. Show-o: One single transformer to unify multimodal understanding and generation. In *ICLR*, 2025. 2, 3, 7
- [72] Jinheng Xie, Zhenheng Yang, and Mike Zheng Shou. Show-o2: Improved native unified multimodal models. *arXiv preprint arXiv:2506.15564*, 2025. 6, 7, 8, 1, 2
- [73] Rongchang Xie, Chen Du, Ping Song, and Chang Liu. MUSE-VL: modeling unified VLM through semantic discrete encoding. *arXiv preprint arXiv:2411.17762*, 2024. 6, 7, 1

- [74] Wulin Xie, Yi-Fan Zhang, Chaoyou Fu, Yang Shi, Bingyan Nie, Hongkai Chen, Zhang Zhang, Liang Wang, and Tieniu Tan. Mme-unify: A comprehensive benchmark for unified multimodal understanding and generation models. *arXiv preprint arXiv:2504.03641*, 2025. [1](#)
- [75] Minhao Xiong, Zichen Wen, Zhuangcheng Gu, Xuyang Liu, Rui Zhang, Hengrui Kang, Jiabing Yang, Junyuan Zhang, Weijia Li, Conghui He, et al. Prune2drive: A plug-and-play framework for accelerating vision-language models in autonomous driving. *arXiv preprint arXiv:2508.13305*, 2025. [2](#)
- [76] An Yang, Baosong Yang, Beichen Zhang, Binyuan Hui, Bo Zheng, Bowen Yu, Chengyuan Li, Dayiheng Liu, Fei Huang, Haoran Wei, Huan Lin, Jian Yang, Jianhong Tu, Jianwei Zhang, Jianxin Yang, Jiaxi Yang, Jingren Zhou, Junyang Lin, Kai Dang, Keming Lu, Keqin Bao, Kexin Yang, Le Yu, Mei Li, Mingfeng Xue, Pei Zhang, Qin Zhu, Rui Men, Runji Lin, Tianhao Li, Tingyu Xia, Xingzhang Ren, Xuancheng Ren, Yang Fan, Yang Su, Yichang Zhang, Yu Wan, Yuqiong Liu, Zeyu Cui, Zhenru Zhang, and Zihan Qiu. Qwen2.5 technical report. *arXiv preprint arXiv:2412.15115*, 2024. [2](#)
- [77] Ling Yang, Zhilong Zhang, Yang Song, Shenda Hong, Runsheng Xu, Yue Zhao, Wentao Zhang, Bin Cui, and Ming-Hsuan Yang. Diffusion models: A comprehensive survey of methods and applications. *ACM computing surveys*, 56(4): 1–39, 2023. [2](#)
- [78] Xiang Yue, Yuansheng Ni, Tianyu Zheng, Kai Zhang, Ruoqi Liu, Ge Zhang, Samuel Stevens, Dongfu Jiang, Weiming Ren, Yuxuan Sun, Cong Wei, Botao Yu, Ruibin Yuan, Renliang Sun, Ming Yin, Boyuan Zheng, Zhenzhu Yang, Yibo Liu, Wenhao Huang, Huan Sun, Yu Su, and Wenhua Chen. MMMU: A massive multi-discipline multimodal understanding and reasoning benchmark for expert AGI. In *CVPR*, pages 9556–9567. IEEE, 2024. [6](#), [1](#)
- [79] Junyuan Zhang, Bin Wang, Qintong Zhang, Fan Wu, Zichen Wen, Jialin Lu, Junjie Shan, Ziqi Zhao, Shuya Yang, Ziling Wang, et al. Trivia: Self-supervised fine-tuning of vision-language models for table recognition. *arXiv preprint arXiv:2512.01248*, 2025. [1](#)
- [80] Kaichen Zhang, Bo Li, Peiyuan Zhang, Fanyi Pu, Joshua Adrian Cahyono, Kairui Hu, Shuai Liu, Yuanhan Zhang, Jingkang Yang, Chunyuan Li, and Ziwei Liu. Lmms-eval: Reality check on the evaluation of large multimodal models, 2024. [6](#)
- [81] Qintong Zhang, Junyuan Zhang, Zhifei Ren, Linke Ouyang, Zichen Wen, Junbo Niu, Yuan Qu, Bin Wang, Ka-Ho Chow, Conghui He, et al. Docr-inspector: Fine-grained and automated evaluation of document parsing with vlm. *arXiv preprint arXiv:2512.10619*, 2025. [1](#)
- [82] Xinjie Zhang, Jintao Guo, Shanshan Zhao, Minghao Fu, Lunhao Duan, Jiakui Hu, Yong Xien Chng, Guo-Hua Wang, Qing-Guo Chen, Zhao Xu, Weihua Luo, and Kaifu Zhang. Unified multimodal understanding and generation models: Advances, challenges, and opportunities. *arXiv preprint arXiv:2505.02567*, 2025. [1](#)
- [83] Chunting Zhou, LILI YU, Arun Babu, Kushal Tirumala, Michihiro Yasunaga, Leonid Shamis, Jacob Kahn, Xuezhe Ma, Luke Zettlemoyer, and Omer Levy. Transfusion: Predict the next token and diffuse images with one multi-modal model. In *ICLR*, 2025. [3](#), [6](#), [7](#), [1](#)

Flash-Unified: A Training-Free and Task-Aware Acceleration Framework for Native Unified Models

Supplementary Material

A. Experimental Setup

We evaluate FlashU against state-of-the-art (SOTA) unified and specialized models across multimodal understanding and generation tasks.

A.1. Baselines

Following the taxonomy proposed in Show-o2 [72], we classify baselines into three categories:

- **Native Unified Models:** Architectures that integrate understanding and generation within a single framework. We compare against *Show-o2* [72], *VILA-U* [70], *Emu3* [62], *Transfusion* [83], *SynerGen-VL* [33], *Liquid* [69], *D-DiT* [34], and *MUSE-VL* [73].
- **Assembling Tailored Models:** Systems that achieve unification by pipelining specialized experts (e.g., separate LLMs and diffusion models). Baselines include *MetaMorph* [58], *ILLUME* [60], *JanusFlow* [46], *SEED-X* [20], and *TokenFlow-XL* [48].
- **Specialized Generation Models:** To benchmark generation fidelity against domain experts, we include *Hunyuan-DiT* [35], *PixArt- Σ* [3], *SD3-Medium* [18], *Playground v2.5* [32], and *DALL-E 3* [2].

Our primary latency-performance comparison is conducted against open-source native unified models that share architectural similarities with our work, namely *VILA-U* [70], *Show-o2* [72], and *Emu3* [62]. To facilitate a more comprehensive analysis, we present an extended latency-performance comparison with *Liquid* [69], *TokenFlow-XL* [48], and *JanusFlow* [46] in Table 6 and Figure 7 of the Appendix.

A.2. Benchmarks and Datasets

Multimodal Understanding We utilize the `lmms-eval` suite to assess performance across six standard benchmarks:

- **MME** [19]: Evaluates perception and cognition using a strict Yes/No format to decouple reasoning capabilities from instruction-following bias.
- **GQA** [24]: Tests compositional reasoning via scene graph-based queries, requiring the parsing of multi-hop spatial and semantic relationships.
- **MMBench** [41]: Addresses evaluation robustness. It employs a “Circular Evaluation” strategy (shuffling options) to penalize inconsistency and random guessing.
- **MMMU** [78]: Assesses expert-level reasoning across diverse disciplines, utilizing college-level problems that demand subject-matter expertise.

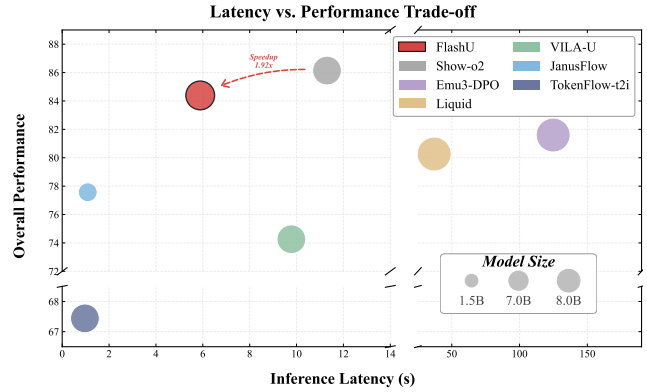


Figure 7. **Latency vs. Performance Trade-off.** Comparison of FlashU against native unified models (*Show-o2*, *VILA-U*, *Emu3-DPO*, *Liquid*) and tailored models (*JanusFlow*, *TokenFlow-t2i*). The x-axis represents inference latency (lower is better), and the y-axis represents overall performance on DPG-Bench (higher is better). Circle sizes denote model parameter counts (1.5B, 7B, 8B).

- **MMStar** [7]: Focuses on visual dependency by filtering out samples answerable via text priors or world knowledge alone (“blind answering”).
- **AI2D** [29]: Examines diagrammatic reasoning, requiring the interpretation of synthetic layouts, symbolic pointers, and process flows in scientific textbook illustrations.

Visual Generation We evaluate alignment and fidelity using two specialized benchmarks designed to test prompt adherence beyond standard metrics:

- **GenEval** [21]: An object-focused evaluation framework that treats generation assessment as a detection problem. It utilizes a fixed set of prompts and pre-trained object detectors to verify specific compositional properties, including *Single/Two Object* presence, *Counting* precision, *Color* attribute binding, and *Spatial Position*.
- **DPG-Bench** [23]: Introduced in ELLA [23], this benchmark employs over 1000 dense, highly descriptive prompts to assess the model’s ability to handle high information loads. It evaluates fine-grained alignment across four specific dimensions: *Global* scene consistency, *Entity* presence, *Attribute* accuracy, and *Relation* (interaction between objects).

B. Implementation Details

In this section, we provide a comprehensive overview of the FlashU inference protocol. We first visually detail the four

Table 6. Latency Comparison on DPG-Bench [23]. Results in gray correspond to vanilla Show-o2. Subscripts indicate the speedup of FlashU. Latency is reported in seconds (s), averaged per sample.

Method	# Params.	Global	Entity	Attribute	Relation	Overall \uparrow	Latency (s) \downarrow
Hunyuan-DiT [35]	1.5B	84.59	80.59	88.01	74.36	78.87	20.1
Playground v2.5 [32]	-	83.06	82.59	81.20	84.08	75.47	7.67
TokenFlow-t2i [48]	7B	72.64	74.72	77.67	83.80	67.44	0.97
JanusFlow [46]	1.5B	81.16	85.16	85.32	91.05	77.57	1.09
VILA-U [70]	7B	89.92	82.73	80.80	87.83	74.26	9.78
Liquid [69]	8B	79.64	87.61	85.24	91.01	80.26	37.05
Emu3-DPO [62]	8B	-	-	-	-	81.60	124.8
Show-o2 [72]	1.5B	87.53	90.38	91.34	90.30	85.02	5.23
+ FlashU (Ours)	1.5B	84.19	89.48	90.98	90.38	84.12	2.82 _{+1.85\times}
Show-o2 [72]	7B	89.00	91.78	89.96	91.81	86.14	11.30
+ FlashU (Ours)	7B	87.79	90.30	89.29	90.30	84.39	5.89 _{+1.92\times}

core acceleration method introduced in our framework, followed by the complete pseudocode governing the dynamic dispatching of these mechanisms and the specific hyperparameter configurations.

B.1. Pseudocode for Unified FlashU Inference

We present the unified inference protocol of FlashU in Algorithm 1. This algorithm demonstrates how the framework dynamically dispatches input queries to task-specific acceleration pathways—switching between iterative generation optimization and understanding optimization within a single unified architecture.

B.2. Hyperparameter Settings

In this section, we provide the specific hyperparameter values used for Generation and Multimodal Understanding (MMU) tasks in Table 7 and Table 8, respectively. Unless otherwise stated, all notation aligns with the definitions in the main text. Baseline and limit constants are defined as follows: T_0 denotes the total inference steps in the baseline Show-o2 model; s_0 represents the base guidance scale; and N_{max} indicates the maximum number of generated tokens for Question Answering (QA) tasks.

C. Parameter Sensitivity Analysis

In this section, we conduct a comprehensive sensitivity analysis to evaluate the impact of key hyperparameters on both inference latency and generation quality. Specifically, we investigate the FFN Pruning Ratio (r_p), Layer Skipping Ratio (r_{LS}), and the Hybrid Threshold (τ) under different guidance strategies. We performed this analysis on the 1.5B model of Show-o2, reporting the DPG-Bench score and predicted speedup relative to the baseline.

Table 7. Hyperparameters for Generation Tasks.

Hyperparameter	Symbol	Value
Total Inference Steps	T	$0.7T_0$
Hybrid Threshold	τ	0.3
FFN Pruning Ratio	r_p	0.20
Layer Skipping Ratio	r_{LS}	0.20
Recalculation Interval	T_{LS}	10
Diffusion Head Cache Interval	\mathcal{T}_{cache}	5
Switching Timestep	t_{switch}	$0.3T$
Low Guidance Scale	s_{low}	$0.75s_0$
High Guidance Scale	s_{high}	s_0

Table 8. Hyperparameters for Multimodal Understanding Tasks.

Hyperparameter	Symbol	Value
Max Generated Tokens	N_{max}	128
Hybrid Threshold	τ	0.3
FFN Pruning Ratio	r_p	0.10
Layer Skipping Ratio	r_{LS}	0.10
Calibration Samples	N_{calib}	20
Recalculation Interval	T_{LS}	10
Shallow layer to prune	L_{prune}	2
Token Pruning Ratio	ρ	0.50

C.1. Impact of FFN Pruning Ratio

As shown in Figure 8, we examine the model’s sensitivity to the FFN Pruning Ratio (r_p) under a fixed configuration of $\tau = 0.3$ and $r_{LS} = 0.2$, utilizing the adaptive guidance strategy.

As r_p increases from 0.1 to 0.5, the speedup exhibits a moderate monotonic increase, rising from $1.82\times$ to $1.94\times$. However, the generation quality, measured by the DPG-Bench score, reveals a distinct non-linear trend. The score

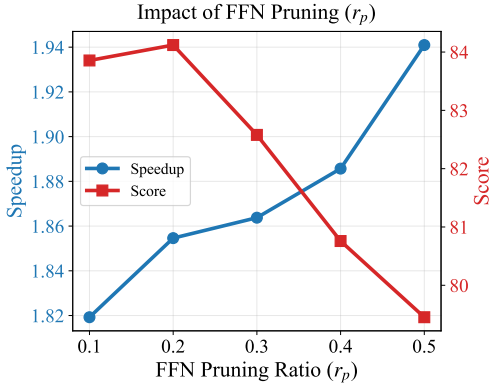


Figure 8. **Sensitivity Analysis of FFN Pruning Ratio.** The trade-off between generation quality (DPG-Bench score) and inference speedup is shown as the FFN pruning ratio (r_p) varies from 0.1 to 0.5.

peaks at 84.12 when $r_p = 0.2$, defining the optimal performance point. Beyond this point, increasing r_p to 0.4 and 0.5 leads to a noticeable degradation in quality, with the score dropping to 79.45 at $r_p = 0.5$. Further aggressive pruning yields diminishing returns in acceleration while significantly compromising visual fidelity.

C.2. Impact of Layer Skipping Ratio

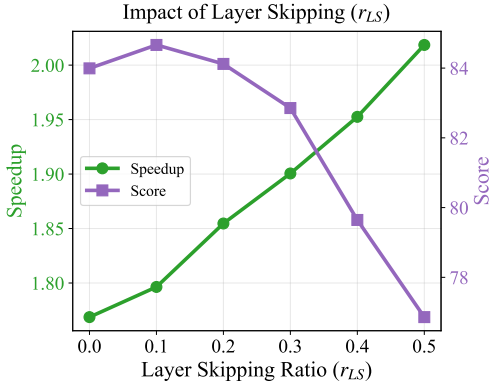


Figure 9. **Sensitivity Analysis of Layer Skipping Ratio.** The relationship between generation quality and speedup across different layer skipping ratios (r_{LS}).

We further analyze the effect of r_{LS} by varying it from 0 to 0.5, while maintaining $r_p = 0.2$ and $\tau = 0.3$.

As shown in Figure 9, the speedup demonstrates a strong positive correlation with r_{LS} , improving significantly from $1.77\times$ achieved at $r_{LS} = 0$ to $2.02\times$ at $r_{LS} = 0.5$. In terms of quality, the model exhibits robustness when $r_{LS} \leq 0.2$, with the DPG-Bench score remaining stable and peaking at 84.66 when $r_{LS} = 0.1$. However, a sharp performance collapse is observed when r_{LS} exceeds 0.3; specifically, at $r_{LS} = 0.5$, the score plummets to 76.86.

Setting r_{LS} to 0.2 establishes the upper bound for layer skipping. Although this setting incurs a negligible quality

trade-off compared to the peak at $r_{LS} = 0.1$, it guarantees a substantial $1.85\times$ acceleration while maintaining robust generative capability.

C.3. Trade-off between Hybrid Threshold and Adaptive Guidance Strategy

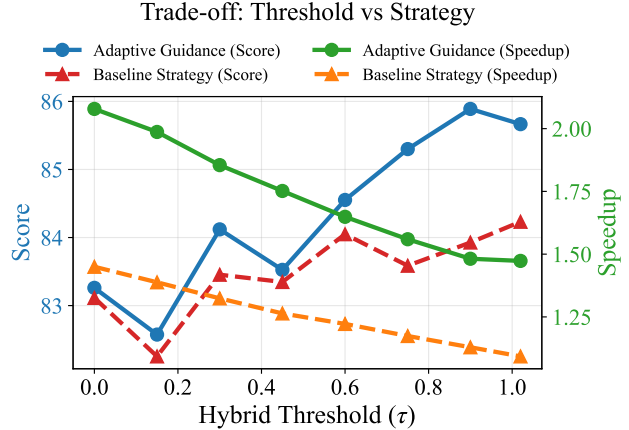


Figure 10. **Comparative Analysis of Hybrid Threshold Strategies.** The efficiency-quality trade-off curves for Adaptive Guidance versus Baseline strategies across different hybrid threshold (τ) values.

We also investigate the trade-off between efficiency and quality by varying the Hybrid Threshold (τ) across two strategies: the proposed Adaptive Guidance with reduced steps and the Baseline as shown in Figure 10.

Both strategies follow a consistent trade-off pattern: as τ increases (retaining more computation), the speedup decreases while the generation quality improves.

The Adaptive Guidance demonstrates a superior Pareto frontier compared to the Baseline. At comparable quality levels, Adaptive Guidance consistently achieves higher speedups. For instance, at $\tau \approx 0.3$, Adaptive Guidance achieves $1.85\times$ speedup versus $1.32\times$ for the Baseline, achieving a score of 84.12 compared to the Baseline’s 83.45. Adaptive Guidance not only accelerates inference but also achieves a higher peak quality. At higher thresholds, such as $\tau \approx 0.9$, Adaptive Guidance reaches a score of 85.89, significantly outperforming the Baseline’s peak performance of roughly 84.23. The combination of Adaptive Guidance and reduced sampling steps proves to be a robust strategy, effectively expanding the efficiency-quality operating envelope beyond the standard baseline.

Based on the analysis above, we adopt the configuration of $r_p = 0.2$, $r_{LS} = 0.2$, and $\tau = 0.3$ with Adaptive Guidance as our default setting. This combination strikes an optimal balance, delivering a $1.85\times$ speedup while maintaining a competitive DPG-Bench score of 84.12.

Algorithm 1 Unified FlashU Inference Protocol

Input: Task Indicator $\mathcal{T} \in \{\text{GEN}, \text{UND}\}$, Input Query Q (Text/Image), Unified Model Weights θ .

Output: Generated Response \mathcal{R} (Image or Text).

Initialize:

```
1: Apply Task-Specific Network Pruning.
2:  $\mathcal{L}_{skip} \leftarrow \emptyset$ ;  $H_{cache} \leftarrow \text{None}$ ;
3:  $\mathcal{R} \leftarrow \emptyset$ .
4: if  $\mathcal{T} == \text{GEN}$  then  $\triangleright$  Pathway A: Image Generation
5:   Parse  $Q$  to initial noise  $z_T$  and text condition  $c$ .
6:   for  $t = T$  to 1 do  $\triangleright$  Iterative Denoising Process
7:      $\triangleright$  Adaptive Guidance
8:      $s_t \leftarrow (t > t_{switch})?s_{low} : s_{high}$ 
9:      $\text{RecalcFlag} \leftarrow (t \bmod K_{skip}) == 0$ 
10:     $h \leftarrow \text{Embed}(z_t, c)$ 
11:    for  $l = 1$  to  $L$  do
12:      if  $l \in \mathcal{L}_{skip}$  and not  $\text{RecalcFlag}$  then
13:        continue
14:       $h_{in} \leftarrow h$ ;  $h \leftarrow \text{SelfAttention}(h, \text{Mask}_{gen})$ 
15:       $h \leftarrow (t > \tau T)?h + \text{FFN}_p(h) : h + \text{FFN}_f(h)$ 
16:      if  $\text{RecalcFlag}$  and  $S(h_{in}, h) > \delta_{th}$  then
17:         $\mathcal{L}_{skip}.add(l)$ 
18:       $\triangleright$  Diffusion Head Cache
19:      if  $(t \bmod K_{cache}) == 0$  then
20:         $H_{cache} \leftarrow \text{DiffHead}(h, t)$ 
21:       $z_{t-1} \leftarrow \text{SchedulerStep}(z_t, H_{cache}, s_t)$ 
22:     $\mathcal{R} \leftarrow \text{VAE-Decode}(z_0)$ 
23:  else if  $\mathcal{T} == \text{UND}$  then  $\triangleright$  Pathway B: MMU
24:    Parse  $Q$  to visual tokens  $X_v$  and text tokens  $X_t$ .
25:    for  $t = 1$  to  $N_{max}$  do  $\triangleright$  Autoregressive Generation
26:       $H \leftarrow \text{Embed}(X_v, X_t, \mathcal{R})$ 
27:      for  $l = 1$  to  $L$  do
28:        if  $l \in \mathcal{L}_{skip}$  and not  $\text{RecalcFlag}$  then
29:          continue
30:         $\triangleright$  Dynamic Visual Token Pruning
31:        if  $l == L_{prune}$  then
32:           $Q, K, V \leftarrow \text{Project}(H)$ 
33:           $S_{imp} \leftarrow \|V\|_2$   $\triangleright$  V-Norm proxy
34:           $\mathcal{I}_{keep} \leftarrow \text{TopK}(S_{imp}, (1 - \rho)|X_v|)$ 
35:           $H \leftarrow \text{Gather}(\mathcal{I}_{keep} \cup X_v, X_t, \mathcal{R})$ 
36:         $H \leftarrow \text{TransformerBlock}(H)$ 
37:       $w_n \leftarrow \text{Sample}(\text{LM-Head}(H[-1]))$ 
38:      break if  $w_n == \text{EOS}$   $\triangleright$  Stopping Criterion
39:       $\mathcal{R}.append(w_{next})$   $\triangleright$  Update context
40: return  $\mathcal{R}$ 
```

D. Component-wise Acceleration Analysis

To understand where FlashU’s acceleration comes from, we conduct fine-grained profiling of the inference time breakdown by component on the 1.5B model. As shown

in Figure 11, the analysis reveals heterogeneous acceleration across components: the Diffusion Head achieves the highest relative speedup (2.82 \times), primarily from iterative caching and adaptive guidance. The LLM forward pass, being the largest component (49% of total time), achieves 1.70 \times speedup through FFN pruning and dynamic layer skipping, contributing the most absolute time savings. Feature Extraction shows moderate acceleration (1.49 \times) via the Hybrid FFN’s lightweight path. VAE decoding remains unchanged, confirming our optimizations introduce no overhead. This component-wise analysis validates that our multi-component optimization strategy effectively eliminates bottlenecks across the entire inference pipeline.

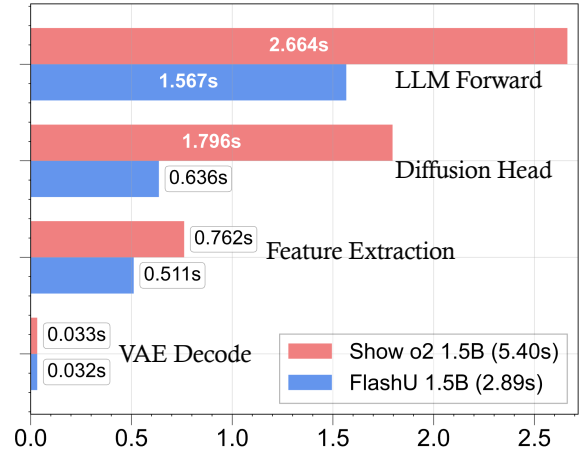


Figure 11. **Component-wise Latency Profiling Analysis.** Inference time breakdown by component for Show o2 and FlashU on the 1.5B model.

E. Additional Qualitative Results

We present additional qualitative results in Figure 12 to further demonstrate the generation capabilities of FlashU. As shown, our method generates high-fidelity and photo-realistic images that accurately align with the given text prompts, effectively preserving the visual quality of the baseline model while significantly accelerating the inference process.



Prompt: An elegant and modern bathroom featuring a sleek, white rectangular bathtub filled with a **froth of soap bubbles**. The bathtub rests upon a **floor of gray, matte tiles** that complement the room's **minimalistic design**. Against the room's far wall stands a large window that frames the **warm, amber hues of a sunset**, casting a **tranquil glow** throughout the space.



Prompt: During the warm glow of a dwindling summer evening, a **particular fussy feline** with distinctive calico markings is perched atop a garden table. The cat, seemingly indifferent to its surroundings, sports a pair of **large, reflective aviator sunglasses** that sit comically upon its small, furry face. Around the cat, there are scattered pots of **blooming flowers**, contributing to the charm of the scene, and in the background, **hints of orange and pink skies** are visible through the foliage.



Prompt: On a rustic wooden table, **three ripe eggplants** with a **glossy royal purple skin** are carefully arranged in a **neat row**. Their plump, oblong shapes complement the table's textured surface, and they **cast soft shadows** in the warm, ambient light. **Nearby, the woven pattern of a tan-colored napkin peeks out from beneath** the vibrant, richly colored vegetables.



Prompt: A curious vessel, with an **architecture reminiscent of a giant green broccoli**, basks in the **bright sunlight**, casting a shimmer across its intricate, leaf-like structures. It **floats serenely in the midst of a vast ocean**, the **water around it sparkling as if sprinkled with diamonds** due to the sun's reflection. The horizon stretches endlessly, with the **clear blue sky meeting the deep azure of the sea** at a distant line.



Prompt: An **ornate silver cosmetics mirror** gracefully positions itself upon a **pristine white marble vanity top**. **Surrounding the mirror** are various high-end makeup products and delicate perfume bottles, **each catching the room's natural light in their uniquely colored glass**. The vanity itself, sleek in design with clean lines, is nestled in a space that feels both modern and timeless.



Prompt: A deep red rose with plush petals sits elegantly **coiled atop an ivory, intricately patterned lace napkin**. The napkin rests on a rustic wooden table that contributes to the charming garden setting. As the late evening sun casts a **warm golden hue** over the area, the **shadows of surrounding foliage dance gently around the rose**, enhancing the romantic ambiance. **Nearby, the green leaves of the garden plants provide a fresh and verdant backdrop** to the scene.



Prompt: **Two multicolored butterflies** with delicate, veined wings gently balance atop a vibrant, orange tangerine in a bustling garden. The tangerine, with its **glossy, dimpled texture**, is situated on a wooden table, contrasting with the **greenery of the surrounding foliage and flowers**. The butterflies, appearing nearly small in comparison, add a touch of grace to the scene, complementing the natural colors of the **verdant backdrop**.



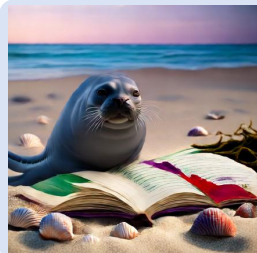
Prompt: On the soft, warm sand of the beach, a fluffy white rabbit with rounded ears is caught in a curious moment, gently placing its paw on the **ribbed surface of a pink scallop shell**. The scallop, slightly open, reveals its smooth interior contrasting with its coarse outer texture, while hues of pink and orange from the setting sun reflect off its surface. There's a **tranquil ocean backdrop** with the gentle ebbing of the tide, and the **fading daylight casts a golden glow** over the scene, highlighting the rabbit's soft fur and the shell's subtle color.



Prompt: A traditional Venetian mask with intricate designs and feather embellishments is placed on a polished wooden table. Next to the mask, there sits a **substantial golden trophy**, shining with reflected light, its **surface etched with small, detailed engravings**. The table and its prestigious items are set against a **deep sepia-toned backdrop** that enhances the objects' visual appeal.



Prompt: In the depths of a **vibrant underwater scene**, a **large, dark red fish** glides gracefully through the water, its scales glistening with the filtered sunlight from above. Surrounding the fish is a **lively coral reef**, bustling with an array of corals in **striking hues of purple, yellow, and green**, their unique and intricate forms providing a **stunning backdrop**. **Tiny, iridescent fish** dart around the nooks of the corals, adding to the dynamic and rich tapestry of marine life inhabiting this tranquil aquatic world.



Prompt: During a tranquil evening, a grey seal with inquisitive eyes explores a **vibrantly illustrated book** left on the **coarse sands of a deserted beach**. The book's pages flutter in the gentle sea breeze, **revealing bursts of purples, greens, and reds**. **Nearby, scattered seashells and washed-up seaweed** provide a natural backdrop to this unusual scene.



Prompt: A small, **teardrop-shaped candle** with a **pale blue hue** graces the surface of a large, **cubic storage box**. The box itself features a textured, glossy white finish and sits squarely in the corner of a room. To the side of the box, there's a stack of **neatly folded towels in varying shades of beige and cream**.

Figure 12. **Qualitative results of text-to-image generation.** We showcase samples generated by FlashU across diverse prompts. The model successfully handles complex descriptions, rendering high-quality textures and correct object placements, demonstrating that our acceleration framework preserves the generative performance of the backbone model.